

# Low mass strange stars and the compact star 1E 1207.4-5209 in the Field Correlator Method

F. I. M. Pereira\*

*Observatório Nacional, Rua Gal. José Cristino 77, 20921-400 Rio de Janeiro RJ, Brazil*

(Dated: July 27, 2021)

We investigate the possible existence of anomalous mass defects in the low mass region of stellar sequences of strange stars. We employ the nonperturbative equation of state derived in the framework of the Field Correlator Method to describe the hydrostatic equilibrium of the strange matter. The large distance static  $Q\bar{Q}$  potential  $V_1$  and the gluon condensate  $G_2$  are the main parameters of the model.

We use the surface gravitational redshift measurements as a probe to determine the ratio  $(\mathcal{P}/\mathcal{E})_C$  at the center of strange stars. For  $V_1 = 0$  and  $G_2 \gtrsim 0.035 \text{ GeV}^4$ , we show that  $(\mathcal{P}/\mathcal{E})_C \simeq 0.262$  and the corresponding redshift  $z_S \simeq 0.47$  are limiting values, at the maximum mass of the highest mass stellar sequence. As a direct application of our study, we try to determine the values of  $V_1$  and  $G_2$  from astrophysical observations of the compact star 1E 1207.4-5209. Due to the uncertainties in the surface redshift determination, we made two attempts to obtain the model parameters. Our findings show that  $(\mathcal{P}/\mathcal{E})_C = 0.073_{+0.024}^{+0.029}$  at 68% confidence,  $V_1 = 0.44 \pm 0.10 \text{ GeV}$  at 90% confidence and  $G_2 = 0.008 \pm 0.001 \text{ GeV}^4$  at 95% confidence in the first attempt; and  $(\mathcal{P}/\mathcal{E})_C = 0.073_{+0.024}^{+0.029} = 0.087 \pm 0.028$  at 71% confidence,  $V_1 = 0.43 \pm 0.085 \text{ GeV}$  at 94% confidence and  $G_2 = 0.0093 \pm 0.00092 \text{ GeV}^4$  at 94% confidence in the second attempt. These values of  $V_1$  and  $G_2$  are in reasonable agreement with the lattice and QCD sum rules calculations. As a consequence of the high values of  $V_1$  and  $G_2$ , the anomalous mass defects of 1E 1207.4-5209 are  $|\Delta_2 M| \simeq 2.56 \times 10^{53} \text{ erg}$  in the first attempt and  $|\Delta_2 M| \simeq 2.94 \times 10^{53} \text{ erg}$  in the second attempt.

PACS numbers: 04.40.Dg, 21.65.Qr, 21.65.Mn

---

\* flavio@on.br, fimpjm@gmail.com

## I. INTRODUCTION

The possibility of anomalous mass defects in compact stars goes back to the works of V. A. Ambartsumyan, G. S. Saakyan and Yu. L. Vartanyan in Refs. [1–5]. Anomalous mass defects would occur at internal stellar energy densities many times greater than the nuclear density ( $\rho_0 \simeq 2.5 \times 10^{14} \text{ g cm}^{-3}$ ). Such stellar configurations, in the presence of external perturbations, would undergo transitions of explosive character, from a metastable state to a stable state, with great amounts of liberated energy. The authors of Refs. [1–5] considered the superdense stellar matter made of a degenerate gas comprising neutrons, protons, hyperons and electrons, at zero temperature.

As baryons are made of quarks, it would be natural to expect unbound quarks to exist in the interior of hyperdense stars. The possibility of hypothetical compact stars made of pure quark matter was then considered by N. Itoh in Ref. [6]. Since the Bodmer-Terazawa-Witten conjecture in Refs. [7–9] the existence of the strange quark matter (SQM), made of an equal number of up, down and strange quarks, has been subject of a lot of theoretical studies, experimental investigations in terrestrial laboratories, and in observational studies of astrophysical phenomena.

The properties of the SQM in the phase diagram, at small temperatures and large densities, were not completely known due to the nonperturbative character of quantum chromodynamics (QCD). Within this scenario the Nambu-Jona-Lasinio Model in Refs. [10, 11] and the MIT Bag Model in Ref. [12] appeared to describe the properties of quark matter. The Nambu-Jona-Lasinio Model has been used to investigate quark matter properties in compact stars, as in Refs. [13, 14]. It exhibits chiral symmetry breaking, but it has the disadvantage in that neither the quark confinement is explicitly included nor the contribution of gluons to account for the dynamics of the quark confinement is considered.

The MIT Bag Model became one of the most used phenomenological models of quark confinement to describe the cold SQM at finite chemical potentials and to investigate the properties of strange stars, as in Refs. [15–18]. However, the model also has the disadvantage in that the quarks are free particles inside the bag that simulates the confinement. For larger distances, when the confining forces become important, it does not account for the way the quarks conglomerate to form hadrons in the quark-hadron phase transition. In other words, the model does not take into account the  $Q\bar{Q}$  interaction potential and the role of the gluon

condensate to describe the quark confinement. Summarizing, neither Nambu-Jona-Lasinio Model nor MIT Bag Model naturally include the dynamics of quark confinement from the first principles of QCD.

In another interesting approach, the quark interaction via the Richardson potential (see Ref. [19]), which incorporates the aspects of the asymptotic freedom and quark confinement, has been used to study the properties of strange stars in Ref. [20] and to describe the SQM in the presence of magnetic field in Ref. [21].

Despite the highly nonlinear character of QCD, the inherent difficulties were overcoming by the advent of the nonperturbative equation of state derived, from first principles, in the framework of the Field Correlator Method (FCM) in Ref. [22]. The great advantage of the FCM approach is that it covers the entire phase diagram plane from high temperatures and low densities to low temperatures and high densities. We have made applications of the FCM nonperturbative equation of state to investigate general aspects of strange stars in Ref. [23] and the SQM stability in Ref. [24]. The authors of Ref. [25] have made an application of the method to investigate quark deconfinement transition in neutron stars. More recently, we have also considered the (normal and anomalous) mass defects of strange stars at the maximum masses of the stellar sequences, in Ref. [26].

In the present article, we study the anomalous mass defects of nonrotating strange stars without crust (or bare strange stars) and without internal magnetic field, within the same lines of our previous investigation in Ref. [26]. The mass-radius relations of strange stars with crust, which have been investigated within the MIT Bag Model, are similar to that of neutron stars, as shown in Fig. 8.5 in Ref. [27]. In the FCM, a richer approach with two parameters, the inclusion of a crust requires a more detailed investigation to be considered in future works. In other words, depending on the values of the model parameters, it is not certain that the results obtained with the FCM will present the same features as the ones obtained with the MIT Bag Model. It may be premature the inclusion of a crust because it could mask the values of the FCM model parameters. From now on, strange stars means bare strange stars.

The nonperturbative treatment of the quark-hadron transition at nonzero  $T$  and  $\mu$  in the presence of magnetic field were considered in the framework of the FCM by the authors of Ref. [28]. In the present work we leave the investigation of strange stars with magnetic field to be considered in future works.

We start the work by studying the anomalous mass defects in the first (ascendant) branches of the stellar sequences, which also includes the region of low mass strange stars. To this end, we first use the solutions of the Tolmann-Oppenheimer-Volkov (TOV) equations for the case of constant energy density (see Ref. [29]) to guide our investigation. In this case, the ratio pressure-to-energy density,  $\mathcal{P}_C/\mathcal{E}_C$ , at the center of a star can be expressed in terms of the surface or gravitational redshift (henceforth simply called redshift) of a radiation emitted at a given frequency from the star surface. Thus, we extend this simple idea to find an analogous description of the general case of stars with non-constant energy density profiles.

The new description can be used to study strange stars in the low mass region of stellar sequences. While masses and radii of strange stars and neutron stars are similar in the high mass regions of the mass-radius diagram, the radii of strange stars and neutron stars with similar masses are very different in the low mass region (cf. Fig. 1 in Ref. [30]). On the other hand, masses and radii decrease for large values of the parameters  $V_1$  and  $G_2$  of the FCM nonperturbative equation of state, as shown in Ref. [23]. So, strange stars of low mass are appropriate for investigations in the region of large values of the parameters  $V_1$  and  $G_2$ . As an example of the applicability of our description, we take the astrophysical observations of the compact star 1E 1207.4-5204 (which is a low mass one) to determine the parameters  $V_1$  and  $G_2$ . A detailed investigation, but within the MIT Bag Model, in Ref. [31] indicates that 1E 1207.4-5204 may be a strange star. In Sec. V we also assume the strange star hypothesis to investigate 1E 1207.4-5204 within the FCM.

The presentwork is twofold. First, it considers compact stars as laboratories to determine the important quantities of the cold SQM at very high densities to describe the low  $T$  and high  $\mu$  (or density) region of the QCD phase diagram. On the other side, there are the experiments at RHIC and LHC to investigate the quark-gluon plasma properties in the high temperature region of the phase diagram. Second, on the astrophysical side, it serves to investigate strange stars properties governed by a nonperturbative equation of state provided by the FCM.

The present paper is organized as follows. In Sec. II we recall the FCM main equations to be used in our calculation. In Sec. III we present the equations needed to describe the stellar configurations. Sec. IV is devoted to the general case of strange stars with non-constant internal energy density profile. In Sec. V, we make an attempt to estimate the

model parameters  $V_1$  and  $G_2$  from the observations of the compact star 1E1207.4-5209. Sec. VI is dedicated to the final remarks.

## II. THE NONPERTURBATIVE EQUATION OF STATE AT ZERO TEMPERATURE

Let us recall the main equations of the FCM thermodynamics of quarks (see Refs. [23, 24, 26] for details). The main parameters of the nonperturbative equation of state are the large distance static  $Q\bar{Q}$  potential  $V_1$  and the gluon condensate  $G_2$ . The pressure, energy density and number density of a quark gas at  $T = 0$  are given by

$$p_q = \frac{N_c}{3\pi^2} \left\{ \frac{k_q^3}{4} \sqrt{k_q^2 + m_q^2} - \frac{3}{8} m_q^2 \left[ k_q \sqrt{k_q^2 + m_q^2} - m_q^2 \ln \left( \frac{k_q + \sqrt{k_q^2 + m_q^2}}{m_q} \right) \right] \right\}, \quad (1)$$

$$\begin{aligned} \varepsilon_q = & \frac{N_c}{\pi^2} \left\{ \frac{k_q^3}{4} \sqrt{k_q^2 + m_q^2} + \frac{m_q^2}{8} \left[ k_q \sqrt{k_q^2 + m_q^2} - m_q^2 \ln \left( \frac{k_q + \sqrt{k_q^2 + m_q^2}}{m_q} \right) \right] \right. \\ & \left. + \frac{V_1}{2} \frac{k_q^3}{3} \right\} \end{aligned} \quad (2)$$

and

$$n_q = \frac{N_c}{\pi^2} \frac{k_q^3}{3}, \quad (3)$$

where

$$k_q = \sqrt{(\mu_q - V_1/2)^2 - m_q^2}, \quad (q = u, d, s), \quad (4)$$

$N_c = 3$  is the color number. The total pressure, energy density and particle number density including electrons are given by

$$p = \sum_{q=u,d,s} p_q - \Delta|\varepsilon_{\text{vac}}| + p_e, \quad (5)$$

$$\varepsilon = \sum_{q=u,d,s} \varepsilon_q + \Delta|\varepsilon_{\text{vac}}| + \varepsilon_e, \quad (6)$$

$$n = n_u + n_d + n_s + n_e, \quad (7)$$

where

$$\Delta|\varepsilon_{\text{vac}}| = \frac{11 - \frac{2}{3}N_f}{32}\Delta G_2 \quad (8)$$

is the vacuum energy density difference between confined and deconfined phases (which from now on will be called vacuum energy density),  $N_f = 3$  is the number of flavors, and  $\Delta G_2 \simeq \frac{1}{2}G_2$  as in Refs. [32, 33]. The value of the gluon condensate,  $G_2 = 0.012 \pm 0.006 \text{ GeV}^4$ , has been determined by QCD sum rule techniques by the authors of Ref. [34].

To obtain the numerical equivalence for the MIT Bag Model we take  $\Delta|\varepsilon_{\text{vac}}| = B$  and  $V_1 = 0$ . However, we emphasize that  $\Delta|\varepsilon_{\text{vac}}|$  is a nonperturbative quantity. In the present work, we assume that  $V_1$  and  $G_2$  are constant quantities (i. e., independent on any flavor chemical potential, or density). We also assume that the SQM composition of strange stars satisfies the requirements of chemical equilibrium under the weak interactions and charge neutrality to perform our calculations of the stellar configurations, as in Refs.: [23, 24, 26].

We use the following values for the quark masses:  $m_u = 5 \text{ MeV}$ ,  $m_d = 7 \text{ MeV}$  and  $m_s = 150 \text{ MeV}$ . The equations for the degenerate electron gas contribution are obtained by making the changes:  $N_c \rightarrow 1$ ,  $V_1 \rightarrow 0$ ,  $\mu_q \rightarrow \mu_e$  and  $m_q \rightarrow m_e$ , in Eqs. (1)-(3).

### III. STELLAR CONFIGURATIONS

Stellar configurations are calculated by numerical integration of the hydrostatic equilibrium equations of Tolman-Oppenheimer-Volkov as in Refs. [29, 35] (we come back to these equations in Sec. III B). Of special importance is the total gravitational mass of a compact star (see Ref. [36] for details),

$$M = \int_0^R \varepsilon(r) dv(r), \quad (9)$$

where  $dv(r) = 4\pi r^2 dr$ , which is the mass that governs the Keplerian orbital motion of the distant gravitating bodies around it, as measured by external observers. The baryonic mass (also called rest mass) of a star is  $M_A = m_A N_A$ , where  $m_A$  is the mass per baryon of the baryon specie  $A$ , with the number of baryons given by

$$N_A = \int_0^R n_A(r) e^{\lambda(r)} dv(r), \quad (10)$$

where  $e^{\lambda(r)} = [1 - 2GM(r)/(c^2 r)]^{-1/2}$  is the spatial function of the metric;  $M(r)$  is the mass within a sphere of radius  $r$ , and

$$n_A = \frac{1}{3}(n_u + n_d + n_s) \quad (11)$$

is the equivalent baryon number density. The baryonic mass is the mass that the star would have if its baryon content were dispersed at infinity, with zero kinetic energy. In the case of strange stars (because of the quark confinement),  $N_A$  is the equivalent number of baryons (not quarks). We here assume  $m_A = m_n$  as in our previous works in Refs.: [23, 24, 26].

### A. Mass defects

With the masses  $M$  and  $M_A$  known, we are in a position to calculate the mass defect (which in our notation<sup>1</sup> is minus the binding energy  $E_b$  defined in Refs. [35, 36]) given by

$$\Delta_2 M = M_A - M. \quad (12)$$

The mass defect corresponds to the energy released to aggregate from infinity the dispersed baryonic matter. In the present work, we will consider unstable stellar configuration with  $\Delta_2 M < 0$  (anomalous mass defect). In this case, the stellar configuration has an energy excess with respect to the energy it would have to be a bound system. The star is in a metastable state, it might explode or implode in the presence of an external perturbation.

In order to consider the general aspects of the anomalous mass defects, let us write the differential elements of the total gravitational mass, the equivalent number of baryons, and the baryonic (or rest) mass given by

$$dM(r) = \varepsilon dv(r) \quad (13)$$

$$dN_A(r) = n_A(r) e^{\lambda(r)} dv(r) \quad (14)$$

$$dM_A(r) = m_A dN_A(r). \quad (15)$$

Then we find that

$$\begin{aligned} \frac{dM(r)}{dN_A(r)} &= \frac{\varepsilon(r)}{n_A(r)} e^{-\lambda(r)} \\ &= m(r) \sqrt{1 - 2 \frac{G M(r)}{c^2 r}}. \end{aligned} \quad (16)$$

---

<sup>1</sup> We here follow the notation according to Refs. [1, 2, 4, 37, 38]

We call  $m(r) \equiv \varepsilon(r)/n_A(r)$  the mass-energy per baryon inside the star. On the surface of the star (taking into account that  $e^{-\lambda R} = e^{\phi R}$  at  $r = R$ ) Eq. (16) becomes

$$\begin{aligned} \left. \frac{dM(r)}{dN_A(r)} \right|_{r=R} &= m_R e^{\phi R} \\ &= m_R \sqrt{1 - 2 \frac{GM}{c^2 R}}, \end{aligned} \quad (17)$$

where  $\phi$  is the temporal function of the metric,  $m_R \equiv m(R)$  and  $M \equiv M(R)$  given by Eq. (9).

Fig. 1 shows the general features of the stellar sequence for the given values of the parameters  $V_1$  and  $G_2$ . The point **3** (in the first branch) indicates an intermediate point around  $0.4M_\odot$  in the low mass region, where the mass defect is anomalous (more visible in Figs. 2 and 3). In Fig. 2, the slope of the  $M$  vs.  $N_A$  curve at the point **3** given by Eq. (17) and that of the  $M_A$  vs.  $N_A$  plot are parallel, which means that

$$\begin{aligned} m_R &= m_A e^{-\phi R} \\ &= m_A (1 + z_S), \end{aligned} \quad (18)$$

which is a redshift relation connecting the mass per baryon at the surface of the star with the baryonic mass  $m_A$  taken as a reference mass by a distant observer. Once  $m_A$  is given, we obtain  $m_R$  by measuring  $z_S$ . On the other hand, inside the star, the energy density  $\varepsilon(r)$ , the baryonic number density  $n_A(r)$ , and the baryonic mass per baryon  $m(r)$  decrease from the center to the surface of the star. Thus, the inequalities  $m_C > m_R > m_A$  (where  $m_C \equiv m(0)$ ) hold in the star interior. In other words, there is anomalous mass defect when  $m(r) > m_A \forall r \in [0, R]$ . If  $m_R \rightarrow m_A$  then the point **3** goes to the origin of the  $M$  vs.  $N_A$  plot in Fig. 2 indicating the absence of the anomalous mass defect when  $m_R = m_A$ , in the first branch of the stellar sequence, as shown in Refs. [1–4, 36]. Moreover, for a given equation of state characterized by fixed values of  $V_1$  and  $G_2$ ,  $m_R$  is constant for all stars along the corresponding stellar sequence. The slope  $m_R e^{\phi R}$  in Eq. (17) evolves according to the temporal function of the metric along the stellar sequence, being greater than  $m_A$  at the origin of the sequence and less than  $m_A$  everywhere above the point **3**. Fig. 3 shows the mass defect. We see by simple inspection that  $|\Delta_2 M|$  is maximum at the point **3**.

We have calculated for different values of  $V_1$  and  $G_2$  the maximum values of  $|\Delta_2 M|$  at the point **3** by searching for points where Eq. (18) holds. The results are depicted in



Fig. 4. Each plot starts from the origin ( $\Delta_2 M = 0$ ) and ends at the maximum mass value of  $\Delta_2 M$  calculated in Ref. [26] where the point **3** is located (also satisfying Eq. (18)). In the low mass region (connected by the dotted line)  $|\Delta_2 M|$  is around  $1 \times 10^{53}$  erg. For the sake of comparison, the energies liberated in type Ia Supernovae originated by white dwarf explosions are of the order of  $(1 - 2) \times 10^{51}$  erg. The total energy of the observed neutrinos in the supernova 1987A was found to be around  $\sim 3 \times 10^{53}$  erg. Thus, explosions of strange stars with anomalous mass defects could be a possibility to be considered.

### B. The Tolmann-Oppenheimer-Volkov equations

To simplify our notation let us define the dimensionless radius and mass by

$$\mathcal{X} \equiv \frac{c^2}{GM_\odot} r \quad \text{and} \quad \mathcal{Z} \equiv \frac{M(r)}{M_\odot}, \quad (19)$$

where  $M(r)$  is the mass within the sphere of radius  $r$ ; and  $GM_\odot/c^2 \simeq 1.5$  km. Thus, the TOV equations are given by

$$\frac{d\mathcal{Z}}{d\mathcal{X}} = \eta \mathcal{X}^2 \mathcal{E}, \quad (20)$$

$$\frac{d\mathcal{P}}{d\mathcal{X}} = - \frac{(\mathcal{E} + \mathcal{P})(\mathcal{Z} + \eta \mathcal{X}^3 \mathcal{P})}{\mathcal{X}^2 (1 - 2 \mathcal{Z}/\mathcal{X})}, \quad (21)$$

where  $\eta \equiv 4\pi (GM_\odot/c^2)^3/M_\odot c^2 \simeq 0.03628 \text{ fm}^3 \text{ GeV}^{-1}$ . The redshift of the spectral lines emitted from the star surface is given by

$$z_S = \frac{1}{\sqrt{1 - 2 \mathcal{Z}_R/\mathcal{X}_R}} - 1, \quad (22)$$

where  $\mathcal{X}_R \equiv \mathcal{X}(r = R)$  and  $\mathcal{Z}_R \equiv \mathcal{Z}(\mathcal{X}_R)$ .

As the redshift has an important role in the present work, let us explore some properties which will be important in the sequel. For finite values of  $\varepsilon_C$  and  $p_C$  at the center of the star<sup>2</sup> we find

$$\left. \frac{d\mathcal{P}(\mathcal{X})}{d\mathcal{X}} \right|_{\mathcal{X}=0} = 0. \quad (23)$$

---

<sup>2</sup> Where  $\mathcal{Z}(\mathcal{X})/\mathcal{X} \rightarrow 0$  when  $\mathcal{X} \rightarrow 0$ .

At the star surface where energy the density is  $\mathcal{E}_R$  and  $\mathcal{P}_R = 0$  we have

$$\begin{aligned} \frac{1}{\mathcal{E}_R} \frac{d\mathcal{P}(\mathcal{X})}{d\mathcal{X}} \Big|_{\mathcal{X}=\mathcal{X}_R} &= - \frac{\mathcal{Z}_R / \mathcal{X}_R}{\mathcal{X}_R [1 - 2 \mathcal{Z}_R / \mathcal{X}_R]} \\ &= - \frac{z_S^2 + 2 z_S}{2 \mathcal{X}_R} \\ &= - \frac{(z_S^2 + 2 z_S)^2}{4 \mathcal{Z}_R (1 + z_S)^2}. \end{aligned} \quad (24)$$

These expressions are of general validity for constant and non-constant energy densities. The right hand sides of Eqs. (24) are observables quantities directly given in terms of  $z_S$  and the dimensionless radius  $\mathcal{X}_R$  or mass  $\mathcal{Z}_R$ .

### C. Constant energy density

In the case  $\mathcal{E} \equiv \mathcal{E}_C = \text{cte.}$  (see Ref. [29]) we find that

$$\mathcal{Z} = \frac{1}{3} \eta \mathcal{E}_C \mathcal{X}^3, \quad (25)$$

$$\begin{aligned} \mathcal{P} &= \mathcal{E}_C \frac{\sqrt{1 - 2\mathcal{Z}/\mathcal{X}} - \sqrt{1 - 2\mathcal{Z}_R/\mathcal{X}_R}}{3 \sqrt{1 - 2\mathcal{Z}_R/\mathcal{X}_R} - \sqrt{1 - 2\mathcal{Z}/\mathcal{X}}} \\ &= \mathcal{E}_C \frac{\sqrt{1 - \frac{2}{3} \eta \mathcal{E}_C \mathcal{Z} \mathcal{X}^2} - \sqrt{1 - \frac{2}{3} \eta \mathcal{E}_C \mathcal{Z}_R \mathcal{X}_R^2}}{3 \sqrt{1 - \frac{2}{3} \eta \mathcal{E}_C \mathcal{Z}_R \mathcal{X}_R^2} - \sqrt{1 - \frac{2}{3} \eta \mathcal{E}_C \mathcal{Z} \mathcal{X}^2}}. \end{aligned} \quad (26)$$

The redshift is now given by

$$z_S = \frac{1}{\sqrt{1 - \frac{2}{3} \eta \mathcal{E}_C \mathcal{Z}_R \mathcal{X}_R^2}} - 1. \quad (27)$$

Taking  $\mathcal{X} = 0$  in Eqs. (26), the ratio  $\mathcal{P}_C/\mathcal{E}_C$  at the center of the star is given by

$$\frac{\mathcal{P}_C}{\mathcal{E}_C} = \frac{z_S}{2 - z_S}. \quad (28)$$

The equation of state at the center of a compact star with constant energy density can be obtained by direct redshift measurements. Thus, we can use the redshift as a probe to give us the equation of state at the center of a compact star in the  $\mathcal{E} \equiv \mathcal{E}_C = \text{cte.}$  approximation. For finite  $\mathcal{P}_C/\mathcal{E}_C \geq 0$ , we note that  $z_S < 2$ , according to Eq. (11.6.20) in Ref. [39]. Additionally, we note that the above solution for  $\mathcal{P}_C/\mathcal{E}_C$  does not depend on the equation of state of the

nuclear or strange matter. This is an interesting property to be used to test theoretical models.

Low mass compact stars have been commonly accepted as the ones with masses lower than the solar mass, and characterized by almost constant internal energy density profiles. The masses of low mass strange stars can be calculated by the Newtonian approximation  $M \simeq (4\pi/3)\varepsilon_S R^3$ , where  $\varepsilon_S$  is the surface energy density, as in Ref. [27]. However, not all low mass compact stars can be approximated by constant internal energy density profiles, as we show in Sec. V. For instance, for certain values of the FCM parameters  $V_1$  and  $G_2$ , the shape of the energy density may present a remarkable change from the center to the surface of the star. In this case, we do not have an analogous prescription to the one given in Eq. (28). However, we can explore the behavior of the theoretical dependence of  $(\mathcal{P}/\mathcal{E})_C$  on  $z_S$  to find a corresponding expression for the case of non-constant energy density profile.

#### IV. $(\mathcal{P}/\mathcal{E})_C$ FOR NON-CONSTANT ENERGY DENSITY

Let us now try to build a representation for  $(\mathcal{P}/\mathcal{E})_C$  to simulate a general case when the energy density is not constant. To this end, we first generate many (theoretical) stellar sequences, each one for a fixed pair of parameters  $(V_1, G_2)$ . The plots of the corresponding ratios  $(\mathcal{P}/\mathcal{E})_C$  vs.  $z_S$  are shown in Fig. 5. We observe that all curves that start very close together from the origin, in a thin bundle of lines, deviate from the initial direction at certain points along the bundle resembling a "cockatiel crest" at the upper parts of the figure. Moreover, the deviation points, each one corresponding to a pair  $(V_1, G_2)$ , are located at the maximum masses of the corresponding stellar sequences. The lines of the "crest" in the second branches of the stellar sequences (such as the one with the point **2**, in Fig. 1) are of no interest in the present work. So, removing the lines of the "crests" at the points of maximum masses, we obtain a thin cloud of aligned points which converge in the low redshift region (say,  $z_S \lesssim 0.1$ ) to the constant energy density solution given by Eq. (28), as shown in Fig. 6.

The next step is to represent the cloud of points by the interpolating curve given by

$$\left(\frac{\mathcal{P}}{\mathcal{E}}\right)_C = y \left(1 - \frac{9}{8}y + 2y^2\right) \quad (29)$$

where  $y \equiv \mathcal{P}_C/\mathcal{E}_C$  is the constant energy density solution given by Eq. (28). In Fig. 6, the

solid line shows the interpolating curve extrapolated to higher redshifts to become visible. The second and third coefficients on the right hand side of Eq. (29) were initially determined by best-fitting methods (see Refs.: [40, 41]) and then rounded in order to give an error estimate  $\lesssim 4\%$  (the best we obtained after many attempts!) at an intermediate redshift range, and zero errors at zero redshift and at the maximum mass redshift, as shown in Figs. 7 and 8. The fractional error of  $(\mathcal{P}/\mathcal{E})_C$  as function of the redshift and the corresponding error for  $z_S$  in terms of  $(\mathcal{P}/\mathcal{E})_C$  (obtained by inverting Eq. (29)), respectively, are shown in a scale from zero to 100. Thus, by this way, we are able to use a redshift measurement as a probe to estimate  $(\mathcal{P}/\mathcal{E})_C$  at the center of a strange star within the errors shown in Figs. 7 and 8. Of course, this is a model dependent procedure valid for the case of the FCM nonperturbative equation of state we are considering, but with an interesting quasi-model independent feature. An application of Eq. (29) is done in Sec. V to investigate the compact star 1E 1207.4-5209.

Coming back to Fig. 5, the curves at the upper parts of the figure become more and more closer, but never exceed the limiting redshift  $z_S \simeq 0.51$ . On the other hand, depending on the values of  $V_1$ , the values of  $(\mathcal{P}/\mathcal{E})_C$  at the maximum masses along the bundle of curves do not exceed a certain limit whatever the values of  $G_2$  may be, suggesting the existence of an upper limit for  $(\mathcal{P}/\mathcal{E})_C$  and a corresponding limit for  $G_2$ . In order to obtain the limits for  $G_2$ , we have considered the solutions for the cases with  $V_1 = 0$  (which gives the highest "crests"), and  $V_1 = 0.5 \text{ GeV}$  (which gives the lowest "crests"). In Fig. 9, for  $V_1 = 0$  and  $G_2 \gtrsim 0.035 \text{ GeV}^4$ ,  $(\mathcal{P}/\mathcal{E})_{C,c}$  (at the point **c**) becomes constant around 0.262 at  $z_S \simeq 0.47$  as it is indicated by the point **c** in Fig. 10. At this point we have  $\mathcal{Z}_R/\mathcal{X}_R \equiv R_S/(2R) \simeq 0.27$ , where  $R_S = 2GM/c^2$  is the Schwarzschild radius of the star. The mass of the star is  $M \simeq 0.58 M_\odot$  and its radius is  $R \simeq 3.19 \text{ km} \simeq 1.85 R_S$ . For  $V_1 = 0.5 \text{ GeV}$ ,  $(\mathcal{P}/\mathcal{E})_{C,d}$  saturates around 0.24 at  $z_S \simeq 0.44$ , but at a too large value of  $G_2$ , say,  $\gtrsim 2.5 \text{ GeV}^4$  (the point **d** is not shown in Fig. 10). The corresponding mass and radius are  $M \simeq 0.06 M_\odot$  and  $R \simeq 0.34 \text{ km} \simeq 1.92 R_S$ .

Let us now consider the the particular situation given by

$$\begin{aligned} \left(\frac{\mathcal{P}}{\mathcal{E}}\right)_C &= \frac{\mathcal{Z}_R}{\mathcal{X}_R} \\ &= \frac{1}{2} \left[ 1 - \frac{1}{(1+z_S)^2} \right]. \end{aligned} \quad (30)$$

Fig. 9 also shows the plot of the right hand side of Eq. (30) together with the plots of  $\mathcal{P}_C/\mathcal{E}_C$

and  $(\mathcal{P}/\mathcal{E})_C$ . By the logic of Fig. 5 the points of the plot given by Eq. (30) are located on the second branches of the stellar sequences. The point **a** is determined by solving the equation

$$y - \frac{1}{2} \left[ 1 - \frac{1}{(1+z_S)^2} \right] = 0, \quad (31)$$

from which we obtain the root  $z_S \simeq 0.39$  and the corresponding ratio

$$\left( \frac{\mathcal{P}}{\mathcal{E}} \right)_{C, \mathbf{a}} \simeq 0.24. \quad (32)$$

Although the point **a** is on the  $\mathcal{P}_C/\mathcal{E}_C$  plot, the value of  $(\mathcal{P}/\mathcal{E})_{C, \mathbf{a}}$  can also be obtained for certain values of  $V_1$  and  $G_2$ . As a result, the point **a** is on the second branches of the stellar sequences for values of the pair  $(V_1, G_2)$  between  $(V_1 \simeq 0.23 \text{ GeV}, G_2 = 0.001 \text{ GeV}^4)$  and  $(V_1 = 0.5 \text{ GeV}, G_2 \simeq 0.012 \text{ GeV}^4)$  (see the value of the gluon condensate in Ref. [34]). In the case of the FCM the internal energy densities of the stars within these values of  $(V_1, G_2)$  are not necessarily constant along the respective stellar sequences. However, roughly constant energy densities occur for masses and radii very lower than the ones at the maximum mass.

Analogously, by solving the equation

$$y(1 - \frac{9}{8}y + 2y^2) - \frac{1}{2} \left[ 1 - \frac{1}{(1+z_S)^2} \right] = 0, \quad (33)$$

we find the root  $z_S \simeq 0.49$  and the ratio

$$\left( \frac{\mathcal{P}}{\mathcal{E}} \right)_{C, \mathbf{b}} \simeq 0.275 \quad (34)$$

corresponding to the point **b**. This point is located on the second branches of the stellar sequences for  $V_1 = 0$  and  $\forall G_2 \gtrsim 0.035 \text{ GeV}^4$ . The differences between the values of  $(\mathcal{P}/\mathcal{E})_C$  and  $z_S$  at the points **b** and **c** are about (4-5) %; and the differences for the masses, radii and  $\mathcal{Z}_R/\mathcal{X}_R$  are  $\lesssim$  (1-3) %. Thus, for observations with error bars  $\gtrsim$  (4-5) % we can assume that **b**  $\simeq$  **c** (**c** is at the maximum mass) to check, from  $z_S$  measurements, if the ratio  $(\mathcal{P}/\mathcal{E})_{C, \mathbf{c}}$  of an observed strange star candidate is near its maximum value.

## V. THE COMPACT STAR 1E 1207.4-5209

As mentioned earlier, the low mass strange stars are more appropriate to test the applicability of the above theoretical developments. Due to the confinement mechanisms controlled by the parameters  $V_1$  and  $G_2$ , the masses and radii of strange stars could be very small (say,

$M \lesssim 0.5 M_\odot$  and  $R \lesssim 10$  km). We have shown in Fig. 8 of the Ref. [23] that the masses and radii of strange stars decrease with the increase of  $V_1$  and/or  $G_2$ . For instance, the decrease of the maximum mass is pronounced for  $V_1 = 0.5$  GeV and  $G_2 = 0.007$  GeV<sup>4</sup> as shown in Fig. 2 of the Ref. [26]. Thus, large values of the model parameters are compatible with low masses and radii. On the other hand, we must have in mind that not all compact stars are low mass stars and have their masses, radii and redshifts given by the observational data. All these facts make the compact star 1E 1207.4-5209 a good example to test the above method.

The compact star 1E1207.4-5209 is an isolated neutron star (INS) discovered near the center of the supernova remnant (SNR) PKS 1209-51 (also known as G296.5+10.0) by the Einstein observatory, in Ref. [42]. Its age is estimated from the remnant, by the authors of Ref. [43], to be around 7 kys, with an uncertainty of a factor 3. The distance to the remnant is about  $d=1.3 - 3.9$  kpc, as estimated in Ref. [44].

The possible SQM composition of 1E 1207.4-5209 was considered in Ref. [31]. In a mass-radius relation investigation in Ref. [45], the mass, radius and redshift of 1E 1207.4-5209 were determined by independent methods to be  $M = 0.34 \pm 0.09 M_\odot$ ,  $R = 4.2 \pm 0.1$  km and  $z_S = 0.12 - 0.23$ . Assuming the SQM composition of 1E 1207.4-5209 governed by the FCM nonperturbative equation of state, we now try to find the parameters  $V_1$  and  $G_2$  from the given astrophysical data. Because the mass, radius and redshift are related by Eq. (22) we have two independent quantities to determine the parameters. As the redshift measurement is given only within a range, we try to obtain the parameters by following two steps.

First, we take as the central value of the redshift the one calculated from the values of the above mass and radius plus their respective error bars, using Eq. (22). Thus, we here assume  $z_S = 0.15_{-0.048}^{+0.057}$  to be used in our calculation. However, the measurements of  $M$  and  $R$ , which appear in the ratio  $M/R$ , are not sufficient to discriminate the values of  $V_1$  and  $G_2$ . Two compact stars with different masses and radii, but with the same ratio  $M/R$ , have the same redshift. For instance, this would be the case of two stars with the same redshift, one on the lower part of the  $(\mathcal{P}/\mathcal{E})_C$  curve and the other on the upper "crest", as we can observe in Fig. 5. To avoid this ambiguity, we have attempted to explore the right hand side of Eq. (24), by saying that even when the redshifts of two different stars are the same, their radii and/or masses are not. Unfortunately, the values of  $[(dp/dr)/\varepsilon]_{r=R}$  are practically constant (around  $-0.03741$  km<sup>-1</sup>), with a variation of  $\sim 0.003\%$  within the

parameter range, resulting inappropriate to our task. So, in this first attempt to determine the parameters (based only on the values of  $M$ ,  $R$  and  $z_S$ ), we have obtained a large range of values for  $V_1 \in [0, 0.5] \text{ GeV}$  and  $G_2 \in [0.0076, 0.014] \text{ GeV}^4$ , as we see in the  $V_1$  vs.  $G_2$  plot depicted by the solid line in Fig. 11.

In order to narrow the search to get better results, we use the additional observable given by Eq. (29). Briefly summarizing our strategy, we have generated  $N$  random points (with normal distribution, which seems to be a reasonable assumption) within the error bars of the  $M$  and  $R$  determinations in Ref. [45] to calculate the redshift values with which, in turn, through Eq. (29), we generate the corresponding points for  $(\mathcal{P}/\mathcal{E})_C$ . Then, applying the standard methods of data analysis in Refs. [40, 41], we find  $(\mathcal{P}/\mathcal{E})_C = 0.073^{+0.029}_{-0.024}$  at 68% confidence (indicated by the cross **A** in Fig. 12). As a result, within the same strategy (generating new random points within the error bars of  $(\mathcal{P}/\mathcal{E})_C$ ), we have obtained  $V_1 = 0.44 \pm 0.11 \text{ GeV}$  at 90% confidence and  $G_2 = 0.0082 \pm 0.001 \text{ GeV}^4$  at 95% confidence (the cross **A** in Fig. 11). Then, according to these predictions (now taken at the central values of the model parameters), the compact star 1E 1207.4-5209 is characterized by the central pressure  $\mathcal{P}_C \simeq 0.12 \text{ GeV fm}^{-3}$  and energy density  $\mathcal{E}_C \simeq 1.6 \text{ GeV fm}^{-3} \simeq 11 \varepsilon_0$  (where  $\varepsilon_0 \simeq 0.141 \text{ GeV fm}^{-3}$  is the nuclear energy density); the mass per baryon  $m_C \simeq 1.78 \text{ GeV} \simeq 1.89 m_A$  at  $r = 0$  and  $m_R \simeq 1.75 \text{ GeV} \simeq 1.87 m_A$  at  $r = R$ . As a consequence of the high values of  $V_1$  and  $G_2$ , the predicted anomalous mass defect is  $|\Delta_2 M| \simeq 2.56 \times 10^{53} \text{ erg}$ .

Second, let us consider the the redshift range 0.12-0.23 from which we take the redshift  $z_S = 0.175 \pm 0.055$ . Making a similar calculation to that considered in the first step, we find the corresponding observable  $(\mathcal{P}/\mathcal{E})_C = 0.087 \pm 0.028$  at 71% confidence (indicated by the cross **B** in Fig. 12 obtained from Eq. (29). The dashed line in Fig. 11 has the same meaning as the solid line in the first step. By an analogous procedure to narrow our search we obtained  $V_1 = 0.43 \pm 0.085 \text{ GeV}$  at 94% confidence and  $G_2 = 0.0093 \pm 0.00092 \text{ GeV}^4$  at 94% confidence. In this case, the compact star 1E 1207.4-5209 is characterized by the central pressure  $\mathcal{P}_C \simeq 0.17 \text{ GeV fm}^{-3}$  and energy density  $\mathcal{E}_C \simeq 1.95 \text{ GeV fm}^{-3} \simeq 14 \varepsilon_0$ ; the mass per baryon  $m_C \simeq 1.81 \text{ GeV} \simeq 1.93 m_A$  at  $r = 0$  and  $m_R \simeq 1.77 \text{ GeV} \simeq 1.88 m_A$  at  $r = R$ . The corresponding anomalous mass defect is  $|\Delta_2 M| \simeq 2.94 \times 10^{53} \text{ erg}$ . We observe that the results for  $|\Delta_2 M|$  are not in contradiction with the ones shown in Fig. 4. The star 1E 1207.4-5209 is neither at the maximum mass nor at the point **3** of the stellar sequence corresponding to the above values of  $V_1$  and  $G_2$ .

In both steps considered above, it is a remarkable feature of the FCM that the determination of the  $Q\bar{Q}$  interaction potential and the gluon condensate from observations of the star 1E 1207.4-5209 are in good agreement with  $V_1 = 0.5 \text{ GeV}$ , obtained from lattice calculations in Ref. [46], and with  $G_2 = 0.009 \pm 0.007 \text{ GeV}^4$  given by QCD sum rules calculations in Ref. [47], as shown in Fig. 11.

Fig. 13 shows the mass-radius relations up to the maximum masses corresponding to the two determinations of the parameters  $V_1$  and  $G_2$  as well as the location of the star 1E 1207.4-5209 in the M-R diagram. The curve **B** is displaced to the left of the curve **A** because of the error in the redshift assumed in the second step, which does not exactly satisfies Eq. (22).

Another feature of the FCM is that, for increasing values of  $V_1$  and  $G_2$ , the stellar configurations have lower masses and radii (cf. Fig. 2 in Ref. [26]). In this case, it is not true that the Newtonian approximation is valid to calculate masses of strange stars, except in the very low mass regions, compared to the ones at the maximum masses (not the solar mass, as it is commonly accepted), of the stellar sequences. The star 1E 1207.4-5209 is a good example of a low mass compact star with a pronounced variation of the internal energy density profile from  $r = 0$  to  $r = R$ , as shown in Fig. 14.

## VI. FINAL REMARKS

In the present work, we have addressed the question of anomalous mass defects of low mass strange stars in the framework of the Field Correlator Method (FCM). The redshift measurements have played an important role in the determination of the model parameters  $V_1$  and  $G_2$  from astrophysical observations. In the case of the constant energy density solution of the Tolmann-Oppenheimer-Volkov equations, the ratio  $(\mathcal{P}/\mathcal{E})_C$  at the center of a compact star is an important observable quantity that can be determined from redshift measurements. It tells us how the equation of state at  $r = 0$  is.

In the general case, when the energy density is not constant, we have verified that the plots of  $(\mathcal{P}/\mathcal{E})_C$  vs. redshift, for different values of  $V_1$  e  $G_2$ , are concentrated in a thin region with a quasi linear behavior, ranging from the origin to the maximum masses in the first branches of the stellar configurations. This fact has enabled us to build a representation for the ratio  $(\mathcal{P}/\mathcal{E})_C$  in terms of the redshift similar to the one for the case of constant energy density. A remarkable feature of our approach is that the ratio  $(\mathcal{P}/\mathcal{E})_C$  as function of the redshift has



the lowest values with respect to the models of nuclear matter. For instance, we illustrate in Fig.15 the ratio  $(\mathcal{P}/\mathcal{E})_C$  for the Walecka nuclear mean field theory in Refs. [48, 49]. Our preliminary calculations have shown that the values of  $(\mathcal{P}/\mathcal{E})_C \forall z_S \in [0, 0.5]$  are in the intermediate region between the solution for constant energy density and the one corresponding to the SQM in the FCM framework. However, for different values of the coupling constants  $g_\sigma/m_\sigma$  and  $g_\omega/m_\omega$  of the nuclear mean field theory the curves of  $(\mathcal{P}/\mathcal{E})_C$  (in the redshift range we are considering) are not concentrated in a line of points as they are for the FCM. An interesting task to be considered in future works is the investigation of the behavior of the ratio  $(\mathcal{P}/\mathcal{E})_C$  given by other models of nuclear matter in the framework of the mean field theories. Our attempt to determine ratio  $(\mathcal{P}/\mathcal{E})_C$  in terms of the redshift is model dependent, but with an almost model independent feature. It is important to verify if this feature remains valid for other approaches used to describe SQM, as the one considered in terms of the Richardson  $Q\bar{Q}$  potential in Ref. [21].

### ACKNOWLEDGMENTS

This work was done with the support provided by the Ministério da Ciência , Tecnologia e Inovação (MCTI).

- 
- [1] V. A. Ambartsumyan and G. S. Saakyan, Sov. Astron. - AJ **4**, 187 (1960).
  - [2] V. A. Ambartsumyan and G. S. Saakyan, Sov. Astron. - AJ **5**, 601 (1962).
  - [3] V. A. Ambartsumyan and G. S. Saakyan, Sov. Astron. - AJ **5**, 779 (1962).
  - [4] G. S. Saakyan and Yu. L. Vartanyan, Sov. Astron. - AJ **8**, 147 (1964).
  - [5] V. A. Ambartsumyan, Problemes de la Cosmogonie Contemporaine, Editions MIR, Moscou, 1971.
  - [6] N. Itoh, Prog. Theor. Phys. **44**, 291 (1970).
  - [7] A. R. Bodmer, Phys. Rev. D **4**, 1601 (1971).
  - [8] H. Terazawa, INS-Report-**336** (INS, University of Tokyo, Tokyo) May, 1979.
  - [9] E. Witten, Phys. Rev. D **30**, 272 (1984).
  - [10] Y. Nambu, G. Jona-Lasinio, Phys. Rev. **122**, 345 (1961).
  - [11] Y. Nambu, G. Jona-Lasinio, Phys. Rev. **124**, 246 (1961).
  - [12] A. Chodos, R. L. Jaffe, K. Johnson, C. B. Thorne and V. F. Weisskopf, Phys. Rev. D **9**, 3471

- (1961).
- [13] D. P. Menezes and C. Providência, *Phys. Rev. C* **68**, 035804 (2003).
  - [14] D. P. Menezes and C. Providência, *Braz. J. Phys.* **34**, 724 (2004).
  - [15] E. Farhi, R. L. Jaffe, *Phys. Rev. D* **30**, 2379 (1984).
  - [16] C. Alcock, E. Farhi and A. Olinto, *Astrophys. J.* **310**, 261 (1986).
  - [17] P. Haensel, J. L. Zdunik and R. Schaeffer, *Astron. Astrophys.* **160**, 121 (1986).
  - [18] K.Kohri, K. Iida and K. Sato, *Prog. Theor. Phys. Suppl.* **151**, 181 (2003).
  - [19] J. L. Richardson, *Phys. Lett. B* **82**, 272 (1979).
  - [20] M. Dey, I.Bombaci, J. Dey, S. Ray and B. C. Samanta, *Phys. Lett. B* **438**, 123 (1998).
  - [21] M. Sinha, Xu-Guang Huang and A. Sedrakian , *Phys. Rev. D* **88**, 025008 (2013).
  - [22] Yu. A.Simonov, *Ann. Phys.* **323**, 783 (2008).
  - [23] F. I. M. Pereira, *Nucl. Phys. A* **860**, 102 (2011).
  - [24] F. I. M. Pereira, *Nucl. Phys. A* **897**, 151 (2013).
  - [25] D. Logoteta and I. Bombaci, *Phys. Rev. D* **88**, 063001 (2013).
  - [26] F. I. M. Pereira, *Nucl. Phys. A* **953**, 65 (2016).
  - [27] P. Haensel, A. Y. Potenkin and D. G. Yakovlev, *Neutron Stars 1, Equation of State and Structure*, Springer, New York, 2007.
  - [28] Yu. A.Simonov, *Phys. Rev. D* **89**, 054012 (20014).
  - [29] S. L. Shapiro and S. A. Teukolski, *Black Holes, White Dwarfs and Neutron Stars*, John Wiley and Sons, New York, 1983.
  - [30] I. Bombaci, *Proceedings of the MG11 Meeting on General Relativity* . Edited by Hagen Kleinert, Robert T Jantzen. Editor of the Marcel Grossmann Meeting series: Remo Ruffini. Published by World Scientific Publishing Co. Pte. Ltd., 2008, pp. 605-628, September 2008; arXiv: 0809.4228v1 [gr-qc].
  - [31] R. X. Xu, *Mon. Not. R. Astron. Soc.* **356**, 359 (2005).
  - [32] Yu. A.Simonov and M. A. Trusov, *JETP Lett.* **85**, 598 (2007).
  - [33] Yu. A.Simonov and M. A.Trusov, *Phys. Lett. B* **650**, 36 (2007).
  - [34] M. A. Shifman, A. I. Veinstein and V. I. Zakharov, *Nucl. Phys. B* **417**, 385 (1979).
  - [35] N. Glendenning, *Compact Stars, Nuclear Physics, Particle Physics, and Relativity*, Springer, New York, 2000, 2nd ed..
  - [36] Ya. B. Zel'dovich and I. D. Novikov, *Stars and Relativity*, Dover Publications, Inc., Mineola,

- New York, 1996.
- [37] Yu. L. Vartanyan, A. R. Arutyunyan and A. K. Grigoryan, *Astrophysics* **37**, 271 (1994).
  - [38] Yu. L. Vartanyan, A. K. Grigoryan and, G. A. Khachatryan, *Astrophysics* **38**, 152 (1995).
  - [39] S. Weinberg, *Gravitation and Cosmology*, John Wiley & Sons, New York, 1972.
  - [40] P. R. Bevington, *Data Reduction and Error Analysis for the Physical Sciences*, McGraw-Hill Book Company, New York, 1969.
  - [41] P. R. Bevington, D. K. Robinson, *Data Reduction and Error Analysis for the Physical Sciences*, McGraw-Hill Higher Education, New York, 2003.
  - [42] D. J. Helfand and R. H. Becker, *Nature* **307**, 215 (1984).
  - [43] R. S. Roger, D. K. Milne, M. J. Kesteven, K. J. Wellington and R. F. Haynes, *Astrophys. J.* **332**, 940 (1988).
  - [44] E. B. Giacani, G. M. Dubner, A. J. Green, W. M. Goss and B. M. Gaensler, *Astron. J.* **119**, 281 (2000).
  - [45] C. M. Zhang, H. X. Yin, Y. Kojima, H. K. Chang, R. X. Xu, X.-D. Li, B. Zhang and B. Kiziltan, *Mon. Not. R. Astron. Soc.* **374**, 232 (2007).
  - [46] O.Kaczmarek and F. Zantov, arXiv:hep-lat/0506019.
  - [47] B. L. Ioffe and K. Zyablyuk, *Eur. Phys. J. C* **27**, 229 (2003).
  - [48] J. D. Walecka, *Ann. Phys.* **83**, 491 (1974).
  - [49] B. D. Serot and J.D. Walecka, *Advances in Nuclear Physics* **16**, Plenum Press, 1986.

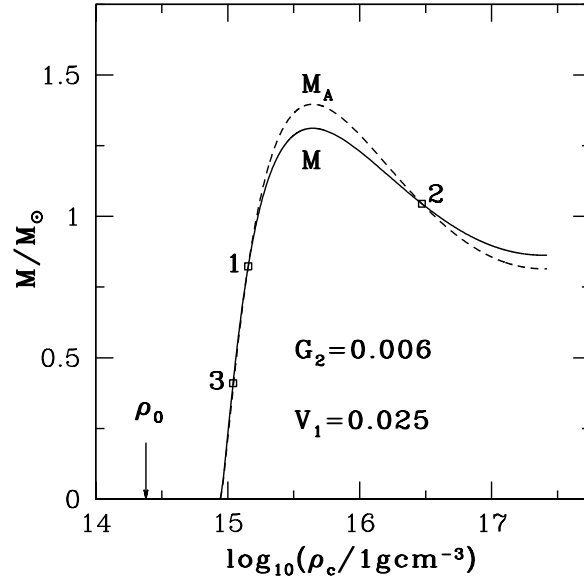


FIG. 1. For the given values of  $G_2$  (in  $\text{GeV}^4$  units) and  $V_1$  (in  $\text{GeV}$  units), gravitational mass  $M$  and baryonic mass  $M_A$  (in units of the solar mass) as functions of the central density. The arrow indicates the nuclear energy density  $\rho_0 \simeq 2.5 \times 10^{14} \text{ g cm}^{-3}$ .

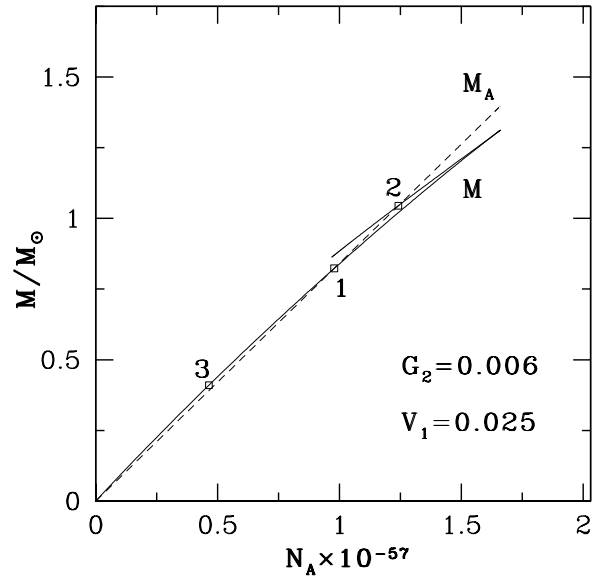


FIG. 2. Same as the previous figure but for gravitational mass  $M$  and baryonic mass  $M_A$  versus baryonic number  $N_A$ . Points **1**, **2** and **3** are in direct correspondence with the ones in Fig. 1.

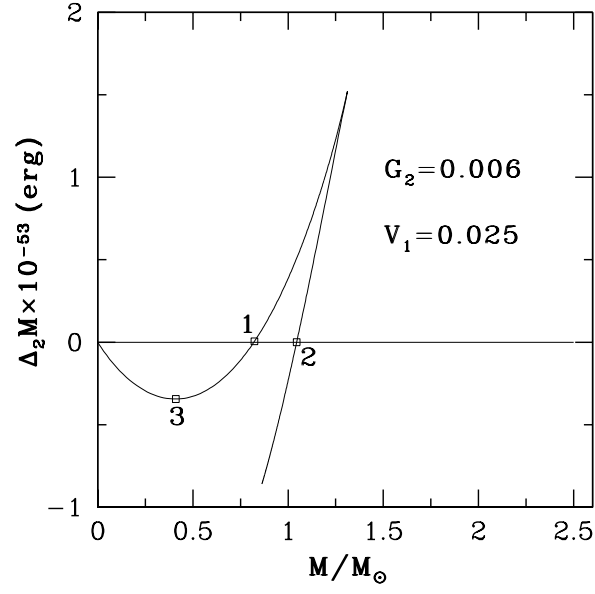


FIG. 3. Same as the previous figures but for mass defect versus gravitational mass  $M$ . Points **1**, **2** and **3** are in direct correspondence with the ones in Figs. 1 and 2.

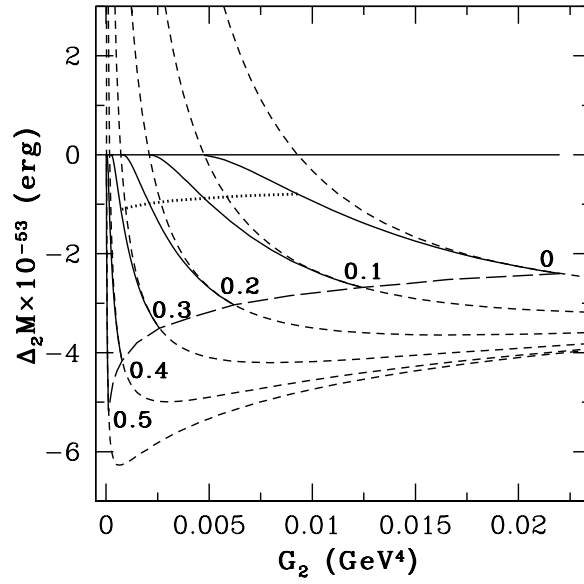


FIG. 4. Mass defect  $\Delta_2 M$  versus  $G_2$  for different values of  $V_1$  between  $V_1 = 0$  and  $V_1 = 0.5$  GeV. The labels correspond to the values of  $V_1$  (in GeV units). *Solid lines*:  $\Delta_2 M$  at the point **3** with  $m_R$  and  $m_A$  satisfying Eq. (18). *Short dashed lines*:  $\Delta_2 M$  at the maximum masses of the stellar configurations (cf. Fig. 4 in Ref. [26]). *Dotted line*:  $\Delta_2 M$  at the point **3** of the low stellar masses ranging from  $M/M_\odot \simeq 0.6$  at  $V_1 = 0$  to  $M/M_\odot \simeq 1.1$  at  $V_1 = 0.3$  GeV. *Long dashed line*: only connecting the points of  $\Delta_2 M$  where the point **3** is at the maximum mass.

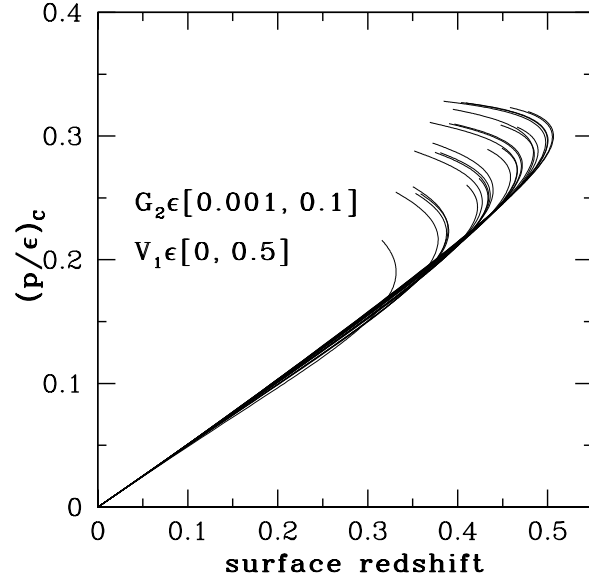


FIG. 5. For the given ranges of  $G_2$  (in  $\text{GeV}^4$  units) and  $V_1$  (in  $\text{GeV}$  units), ratios  $(\mathcal{P}/\mathcal{E})_C$  as function of the redshift. The values of  $V_1$  increase from top to bottom. The values of  $G_2$  increase from bottom to top.



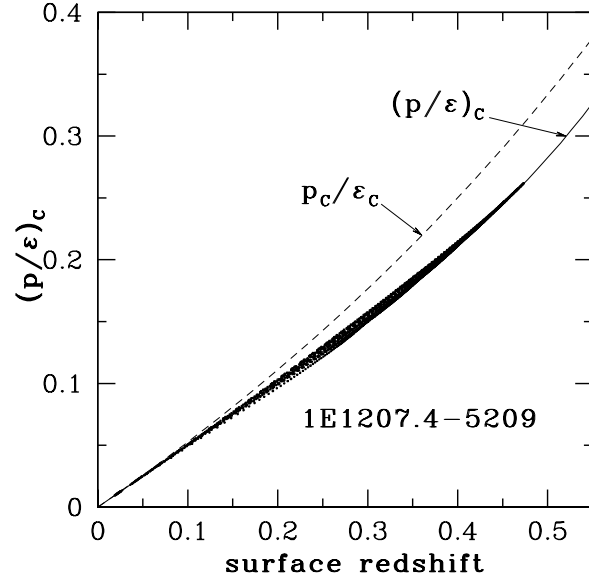


FIG. 6. Same as the previous figure but for the values of  $(\mathcal{P}/\mathcal{E})_C$  ending at the maximum masses of the stellar configurations. *Short dashed line*:  $\mathcal{P}_C/\mathcal{E}_C$  given by Eq. (28). *Solid line*:  $(\mathcal{P}/\mathcal{E})_C$  given by Eq. (29) extrapolated for higher values of the redshift to become visible.

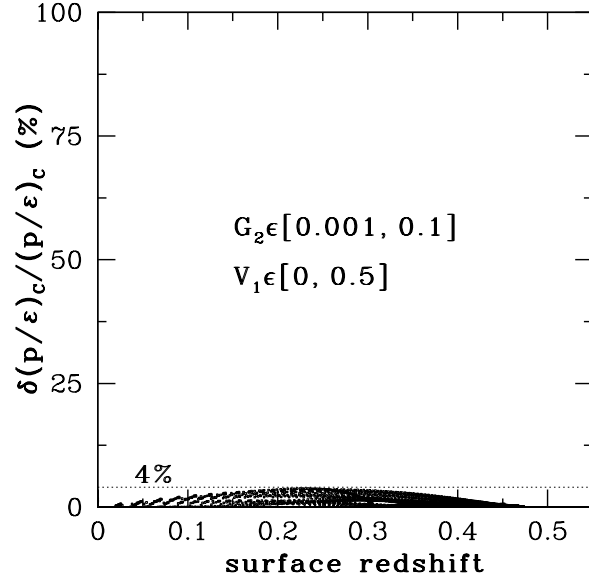


FIG. 7. For the given ranges of  $G_2$  (in  $\text{GeV}^4$  units) and  $V_1$  (in GeV units), fractional error  $\delta(\mathcal{P}/\mathcal{E})_C / (\mathcal{P}/\mathcal{E})_C$  as function of the redshift.

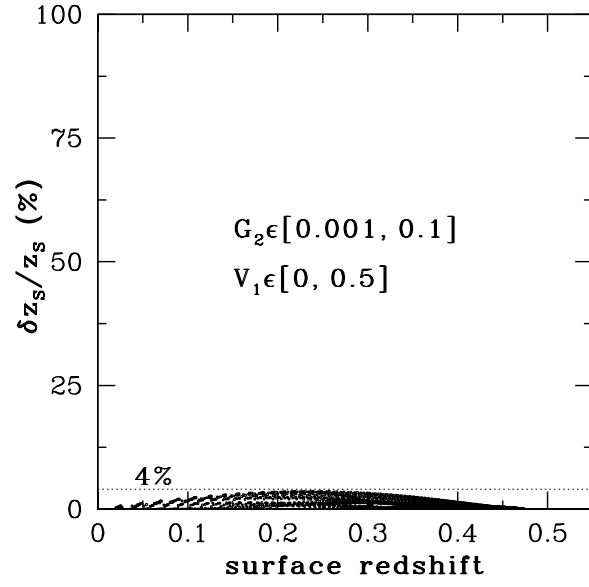


FIG. 8. Same as Fig. 7 but for  $\delta z_s / z_s$ .

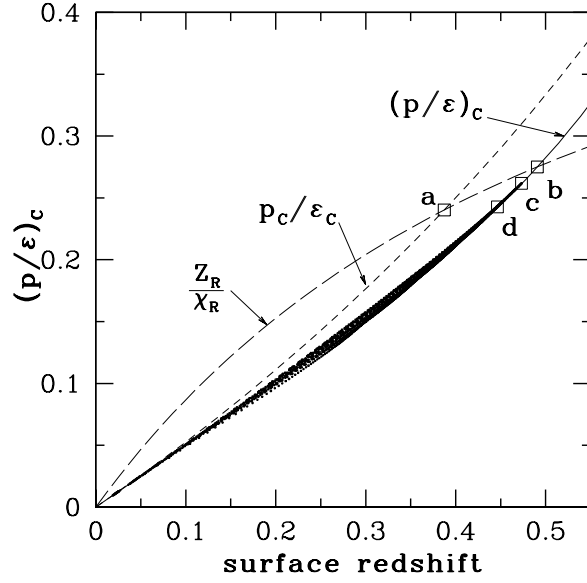


FIG. 9. Same as Fig. 7 but including the  $Z_R/\chi_R$  plot (long dashed line). The point **a** corresponds to Eq. (32) and the point **b** corresponds to Eq. (34). For  $V_1 = 0$ , the point **c** indicates the upper bound  $(\mathcal{P}/\mathcal{E})_{C,c} \simeq 0.262$  and the corresponding redshift  $z_S \simeq 0.47$ . For  $V_1 = 0.5$  GeV, the point **d** indicates the upper bound  $(\mathcal{P}/\mathcal{E})_{C,d} \simeq 0.24$  and the corresponding redshift  $z_S \simeq 0.44$ .

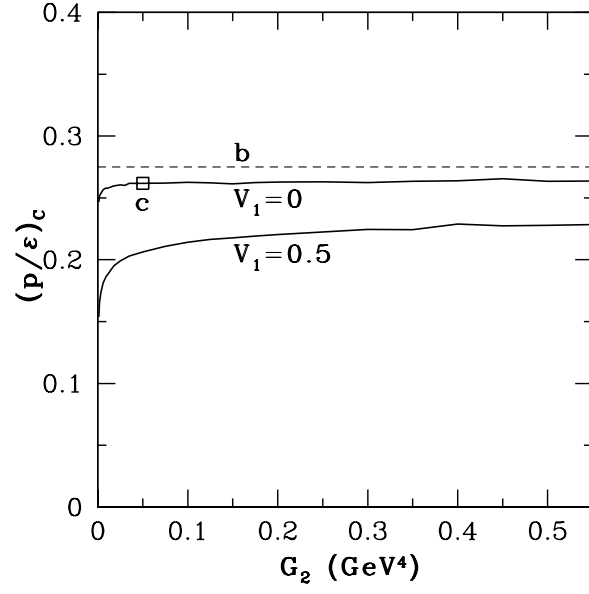


FIG. 10. For increasing values of  $G_2$ , the "constancies" of  $(\mathcal{P}/\mathcal{E})_C$  at **b** and **c**. For  $V_1 = 0.5$  GeV, the "constancy" at the point **d** is not visible in the scale of the figure.

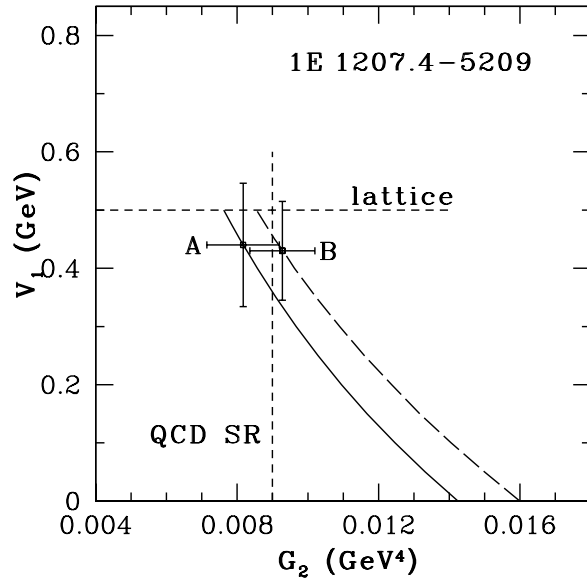


FIG. 11. Solid and long dashed lines show the first and second attempts to determine the model parameters  $V_1$  and  $G_2$  from the mass, radius and redshift measurements provided by the observations of the compact star 1E 1207.4-5209. The crosses **A** and **B** indicate the final results of our narrowed searches for  $V_1$  and  $G_2$ . For comparison, the horizontal short dashed line at  $V_1 = 0.5 \text{ GeV}$  displays the result obtained by lattice calculations, in Ref. [46]. The vertical short dashed line at  $G_2 = 0.009 \text{ GeV}^4$  indicates the central value of  $G_2$  obtained by QCD sum rules (QCD SR) in Ref. [47].

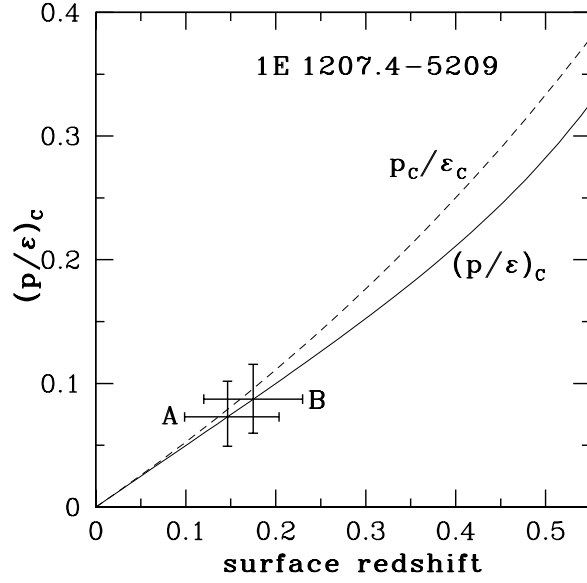


FIG. 12. As in Fig.6 but without the cloud of points. The cross **A** indicates the value of  $(\mathcal{P}/\mathcal{E})_C = 0.073^{+0.029}_{-0.024}$  calculated by Eq. (29) corresponding to the redshift  $z_S = 0.15^{+0.057}_{-0.048}$ . The cross **B** indicates the value of  $(\mathcal{P}/\mathcal{E})_C = 0.087 \pm 0.028$  calculated by Eq. (29) corresponding to the redshift  $z_S = 0.175 \pm 0.055$ .

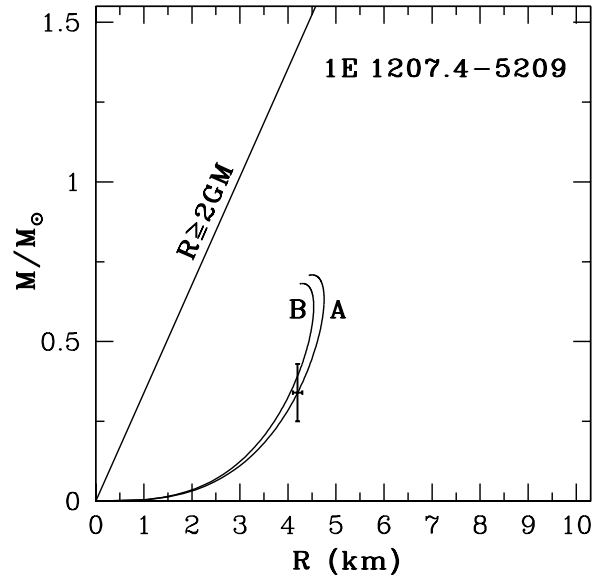


FIG. 13. The cross indicates the mass and radius of the star compact star 1E 1207.4-5209. The curves **A** and **B** are the mass-radius relations corresponding to the values of  $V_1$  and  $G_2$  indicated by the crosses **A** and **B** in Fig. 11, respectively.



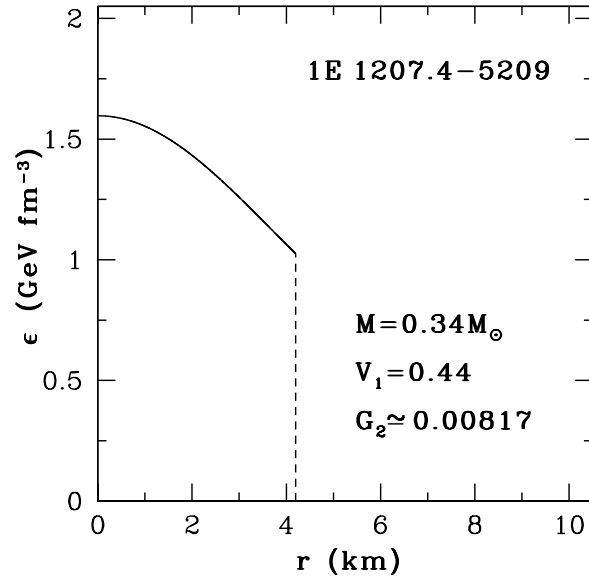


FIG. 14. Internal energy density profile of the compact star 1E 1207.4-5209 versus the radius  $r$ .

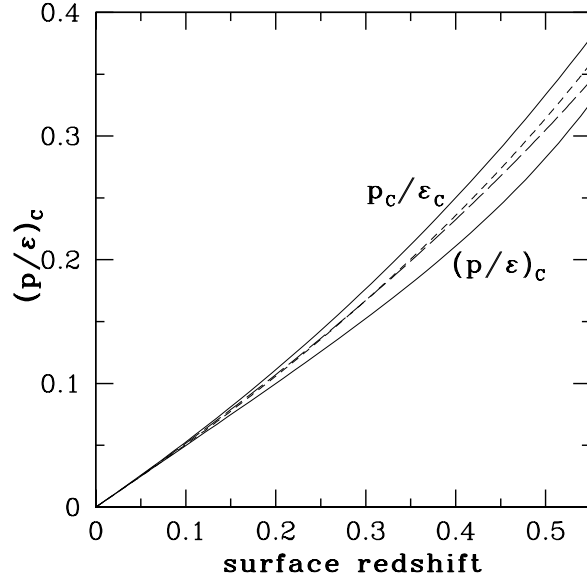


FIG. 15. Ratios pressure-to-energy density at  $r = 0$  as function of the redshift: *Solid lines*,  $\mathcal{P}_C/\mathcal{E}_C$  and  $(\mathcal{P}/\mathcal{E})_C$  given by Eqs.(28) and (29), respectively; *Short dashed line*, for the nuclear mean field theory in Refs.[48, 49] with the coupling constants  $(g_\sigma/m_\sigma)^2 = 11.798 \text{ fm}^2$  and  $(g_\omega/m_\omega)^2 = 8.653 \text{ fm}^2$  fixed to give the bind energy  $E_b = -15.75 \text{ MeV}$  and  $k_F = 1.42 \text{ fm}^{-1}$ ; *Long dashed line*, same as *Short dashed line* but for the arbitrarily chosen values:  $(g_\sigma/m_\sigma)^2 = 15.0 \text{ fm}^2$  and  $(g_\omega/m_\omega)^2 = 12.0 \text{ fm}^2$ .